Strengthening seasonal marine CO_2 variations due to increasing atmospheric CO_2 - Supplementary material

Peter Landschützer[1], Nicolas Gruber[2], Dorothee C. E. Bakker [3], Irene Stemmler[1], Katharina D. Six[1]

[1]*Max Planck Institute for Meteorology, Bundesstr. 53, 20146 Hamburg, Germany*

[2]*Environmental Physics, Institute of Biogeochemistry and Pollutant Dynamics, ETH Zürich, Zürich, Switzerland.*

[3]*Centre for Ocean and Atmospheric Sciences, School of Environmental Sciences, University of East Anglia, Norwich, UK*

1 Neural network estimate - update

Our analysis is based on a previously published and extensively validated global monthly $1^\circ \times 1^\circ$ sea surface $p\mathrm{CO}_2$ product[1], but temporally extended to cover now the period 1982 through 2015. This extension was primarily accomplished by using a newer release of the Surface Ocean Carbon Atlas (SOCAT) dataset, i.e. SOCAT version 4[2]. In this data product, the CO_2 measurements are interpolated in space and time using a 2-step neural network method (SOM-FFN)[3]. The method is extensively described in our previous publications[1,3], but is briefly summarized here again. The surface ocean is first divided into biogeochemical provinces based on common pattern of sea surface temperature (SST)[4], sea surface salinity (S)[5], climatological mixed layer depth (MLD)[6], and climatological sea surface pCO_2[7]. In a second step, the method established a non-linear relation-

ship between environmental drivers and surface ocean CO_2 measurements from the SOCATv4 database[2]. We use the same SST, S and MLD products from step 1 and additionally Globcolour-based chlorophyll-a (http://www.globcolour.info) as well as the NOAA-ESRL marine boundary layer reference dry air mixing ratio of atmospheric CO_2 (https://www.esrl.noaa.gov/gmd/ccgg/mbl/). For the estimated period from 1982 through 2015 we use the same climatological MLD for each year and we estimate chlorophyll-a before the satellite era as the average climatological chlorophyll-a from 1998 through 2015.

Additionally, we use the surface layer data of the $1^\circ \times 1^\circ$ gridded product[8] from the Global Ocean Data Analysis Project version 2 (GLODAPv2)[9], to represent the climatological mean DIC (DIC) and total alkalinity (Alk). Combining the GLODAPv2 data and our long term mean pCO_2, we calculate the climatological mean Revelle factor (γ_{DIC}) using the CO2SYS software[10,11] with the dissociation constants of Mehrbach refitted by Dickson et al.[12,13] as well as the sea surface temperature [4] and the Hadley Center EN4 salinity[5].

Residual analysis The neural network method has been substantially evaluated and validated in past publications[1,3] where it was shown that the method is able to reproduce observations within a small error margin and no systematic bias. Here, we extend this analysis evaluating seasonal mean biases in time in order to test our observation-based data for trends in the seasonal bias that could corrupt our winter-minus-summer trend analysis. Supplementary Figure 1 shows that both annual summer and winter bias are randomly spread around 0 but do show substantial variability. We do, however, not find any temporal trends in the residuals concluding that seasonal trends are

not biased towards, e.g. more densely observed years. This is true for the 4 larger scale latitude bands considered in this manuscript.

Timeseries stations To test the trends in the seasonal cycle derived from our data product, we use observations from the two longest running and most frequently sampled timeseries stations, i.e., from the Station S/Bermuda Atlantic Timeseries Station site in the subtropical North Atlantic (StaS/BATS[14,15] at 31.66°N, 64.16°W) and from the Hawaiian Ocean Timeseries station site in the subtropical North Pacific (HOT[16] at 22.75°N,158.00°W) and calculate the trends in their seasonal (winter-minus-summer) difference. These data, spanning several decades are not included in the SOCATv4 database and thus represent a truly independent estimate in comparison to our $p\mathrm{CO}_2$ data product. At Bermuda we combine the records of Hydrostation S[14] and BATS[15], on the basis of the good agreement between the data at both locations[14,17]. We calculate the sea surface $p\mathrm{CO}_2$ from bottle DIC and alkalinity using the CO2SYS software[10,11] with the dissociation constants of Mehrbach refitted by Dickson et al.[12,13]. At HOT we use the already calculated and available $p\mathrm{CO}_2$ product[16]. We further apply the steps outlined in the methods to the station data, i.e., the separation into thermal and non-thermal components, as well as applying the harmonic-polynomial fit to determine the trend in the seasonal difference as illustrated in Supplementary Figures 2 and 3. Finally, we compute the trends in seasonality of each component from the slope of the linear least square regression line as illustrated in Supplementary Figures 4 and 5.

Additionally, we perform a local comparison between the trends in the seasonal $p\mathrm{CO}_2$ difference from the two timeseries stations above and the SOM-FFN $p\mathrm{CO}_2$ estimate calculated from

the average within the 3x3 degree vicinity of the timeseries location. Locally, we find that trends are indistinguishable with substantial additional uncertainty in the SOM-FFN estimates largely reflecting the stronger year-to-year fluctuations. The results are presented in Table 1.

2 Basin-scale trends in the $p\mathrm{CO}_2$ winter-summer difference

Following our analysis of the global zonal mean trends in the main manuscript, we additionally analyze zonal trends for each basin north of 44°S individually (Supplementary Figure 6). For the Atlantic and Pacific Oceans we find pattern that agree with the global pattern, namely the thermally dominated summer maximum increase (following the sign convention of the main manuscript illustrated as negative winter-minus-summer trend) in the subtropics and the non-thermally dominated winter maximum increase in the high latitudes. We find the largest trends in the Pacific Ocean, whereas the Atlantic Ocean shows stronger meridional variability. Seasonal $p\mathrm{CO}_2$ cycle trends in the northern Indian Ocean are further influenced by the coast. Both the South Pacific and South Indian Ocean further show a decreasing non-thermal seasonal cycle in the subtropics, possibly related to ENSO and the transport of upwelled waters from the equatorial Pacific.

3 Contribution of DIC and the Revelle factor change to the seasonal non-thermal $p\mathrm{CO}_2$ difference

In our theoretical framework we have investigated the uptake of anthropogenic CO_2 and the change in the Revelle factor as the main drivers of the non-thermal seasonal pCO2 increase. Supplementary Figure 7 illustrates zonal mean trends in these 2 components individually. Overall, using the

Table 1: Comparison of trends in the winter-minus-summer difference of $p\mathrm{CO}_2$ at StaS/BATS and HOT with those inferred from the neural network based SOM-FFN estimated $p\mathrm{CO}_2$ in the 3x3 degree area around the respective timeseries location. Note that negative total trends here correspond to an increase in the absolute seasonal difference (following our notation of the main text). Data from the timeseries stations are not included in SOCATv4 used to construct the SOM-FFN estimate

	StaS/BATS	SOM-FFN at StaS/BATS	HOT	SOM-FFN at HOT
Total [μatm/decade]	-1.5$\pm$1.1	-1.5$\pm$1.8	-3.8$\pm$2.4	0.2$\pm$1.8
Thermal [μatm/decade]	-7.2$\pm$1.7	-7.0$\pm$ 2.3	-4.7$\pm$2.0	-2.2$\pm$3.0
Non-thermal [μatm/decade]	3.6$\pm$2.3	4.2$\pm$3.2	0.7$\pm$2.6	2.2$\pm$2.8

theoretical framework we find that, over the past 34 years, the expected contribution of the anthropogenic uptake of CO_2 roughly equals two thirds of the total expected non-thermal increase in the seasonal difference, with the remaining one third explained by changes in the ocean buffer capacity (Supplementary Figure 8).

4 Basin-scale non-thermal pCO_2 seasonal difference framework

Revelle factor changes and the uptake of anthropogenic carbon do not occur at equal strength everywhere in the global ocean. We therefore test our estimated increase in the seasonal non-thermal pCO_2 cycle against our theoretical framework for each major ocean basin individually (Supplementary Figure 9). As identified for the global ocean we find less agreement south of the equator in the subtropics, particularly in the Pacific Ocean and the Indian Ocean, where the neural network-based pCO_2 estimates - unlike the theoretical framework - suggest a decreasing seasonal cycle. In the northern hemisphere the poleward increase in trends is captured both in the Pacific and the Atlantic Ocean though with a much stronger trend in the high latitude North Pacific, suggesting that other factors, e.g. circulation or biology play a major role there.

1. Landschützer, P., Gruber, N. & Bakker, D. C. E. Decadal variations and trends of the global ocean carbon sink. *Global Biogeochemical Cycles* **30**, 1396–1417 (2016). URL `http://dx.doi.org/10.1002/2015GB005359`.

2. Bakker, D. C. E. *et al.* A multi-decade record of high-quality fCO_2 data in version 3 of the Surface Ocean CO_2 Atlas (SOCAT). *Earth System Science Data* **8**, 383–413 (2016). URL

http://www.earth-syst-sci-data.net/8/383/2016/.

3. Landschützer, P. *et al.* A neural network-based estimate of the seasonal to inter-annual variability of the Atlantic Ocean carbon sink. *Biogeosciences* **10**, 7793–7815 (2013).

4. Reynolds, R. W., Rayner, N. A., Smith, T. M., Stokes, D. C. & Wang, W. An improved in situ and satellite sst analysis for climate. *Journal of Climate* **15**, 1609–1625 (2002).

5. Good, S. A., Martin, M. J. & Rayner, N. A. EN4: quality controlled ocean temperature and salinity profiles and monthly objective analyses with uncertainty estimates. *Journal of Geophysical Research: Oceans* **118**, 6704–6716 (2013).

6. de Boyer Montegut, C., Madec, G., Fischer, A. S., Lazar, A. & Iudicone, D. Mixed layer depth over the global ocean: An examination of profile data and a profile-based climatology. *Journal of Geophysical Research* **109**, C12003 (2004).

7. Takahashi, T. *et al.* Climatological mean and decadal change in surface ocean pCO_2, and net sea-air CO_2 flux over the global oceans. *Deep-Sea Research II* **56**, 554–577 (2009).

8. Lauvset, S. K. *et al.* A new global interior ocean mapped climatology: The $1^\circ \times 1^\circ$ GLODAP version 2. *Earth System Science Data* **8**, 325–340 (2016). URL http://www.earth-syst-sci-data.net/8/325/2016/.

9. Olsen, A. *et al.* The Global Ocean Data Analysis Project version 2 (GLODAPv2) – An internally consistent data product for the world ocean. *Earth System Science Data* **8**, 297–323 (2016). URL http://www.earth-syst-sci-data.net/8/297/2016/.

10. Lewis, E. & Wallace, D. W. R. *Program Developed for CO_2 System Calculations, ORNL/CDIAC-105*. Carbon Dioxide Information Analysis Center, Oak Ridge National Laboratory, U.S. Department of Energy, Oak Ridge, Tennessee. (1998). URL `http://cdiac.ornl.gov/oceans/co2rprt.html`.

11. Van Heuven, S., Pierrot, D., Rae, J. W. B., Lewis, E. & Wallace, D. W. R. *MATLAB Program Developed for CO_2 System Calculations. ORNL/CDIAC-105b.* Carbon Dioxide Information Analysis Center, Oak Ridge National Laboratory, U.S. Department of Energy, Oak Ridge, Tennessee. (2011).

12. Mehrbach, C., Culberson, C. H., Hawley, J. E. & Pytkowicz, R. M. Measurement of the apparent dissociation constants of carbonic acid in seawater at atmospheric pressure. *Limnology and Oceanography* **18**, 897–907. (1973).

13. Dickson, A. G. & Millero, F. J. A comparison of the equilibrium constants for the dissociation of carbonic acid in seawater media. *Deep-Sea Research* **34**, 1733–1743 (1987).

14. Gruber, N., Keeling, C. D. & Bates, N. R. Interannual variability in the North Atlantic ocean carbon sink. *Science* **298**, 2374–2378 (2002).

15. Bates, N. R. Multi-decadal uptake of carbon dioxide into subtropical mode water of the North Atlantic ocean. *Biogeosciences* **9**, 2649–2659 (2012).

16. Dore, J. E., Lukas, R., Sadler, D. W. & Church, D. M., M. J.and Karl. Physical and biogeochemical modulation of ocean acidification in the central North Pacific. *Proc Natl Acad Sci USA* **106**, 12235–12240. (2009).

17. Phillips, H. E. & Joyce, T. M. Bermuda's tale of two time series: Hydrostation "s" and bats. *J. Phys. Oceanogr.* **37**, 554–571 (2006).

Figure 1 Residuals as a function of time for winter (left column) and summer (right column) seasons for the 4 latitude bands considered in the main manuscript.

Figure 2 (a) total (b) thermal and (c) non-thermal $p\mathrm{CO}_2$ based on surface ocean measurements at the Bermuda Atlantic Timeseries Station (BATS) and Hydrostation S combined records marked as dots. The solid lines illustrate the polynomial fit to the data.

Figure 3 (a) total (b) thermal and (c) non-thermal $p\mathrm{CO}_2$ based on surface ocean measurements at the Hawaiian Ocean Timeseries Station (HOT) marked as dots. The solid lines illustrate the polynomial fit to the data.

Figure 4 Annual winter-minus-summer difference (dots) and linear regression lines of (a) the total $p\mathrm{CO}_2$, (b) the thermal $p\mathrm{CO}_2$ component and (c) the non-thermal $p\mathrm{CO}_2$ components for the the Bermuda Atlantic Timeseries Station (BATS) and Hydrostation S combined records.

Figure 5 Annual winter-minus-summer difference (dots) and linear regression lines of (a) the total $p\mathrm{CO}_2$, (b) the thermal $p\mathrm{CO}_2$ component and (c) the non-thermal $p\mathrm{CO}_2$ components for the Hawaiian Ocean Timeseries Station (HOT).

Figure 6 Zonal trend in the winter-minus-summer difference for each major ocean basin individually. Negative trends largely indicate where the thermal component (blue) dominates the increase in seasonal difference (black), whereas positive trends largely indicate

where the non-thermal (red) component dominates the increase in seasonality. Stars further indicate the observation-based (gray, red, blue) trend from timeseries stations at Bermuda and Hawaii.

Figure 7 Zonal mean trends in (a) the Revelle factor (γ_{DIC}) and (b) the surface ocean DIC over the past 34 years.

Figure 8 Zonal mean contributions of changes in the Revelle factor and the uptake of anthropogenic carbon to the expected non-thermal $p\mathrm{CO}_2$ seasonal difference trend based on equation 10 of the main manuscript.

Figure 9 Comparison between the neural network based non-thermal (red) $p\mathrm{CO}_2$ seasonal difference trend with the theroretical framework (dashed green line) based on equation 10 of the main manuscript for each major ocean basin individually.

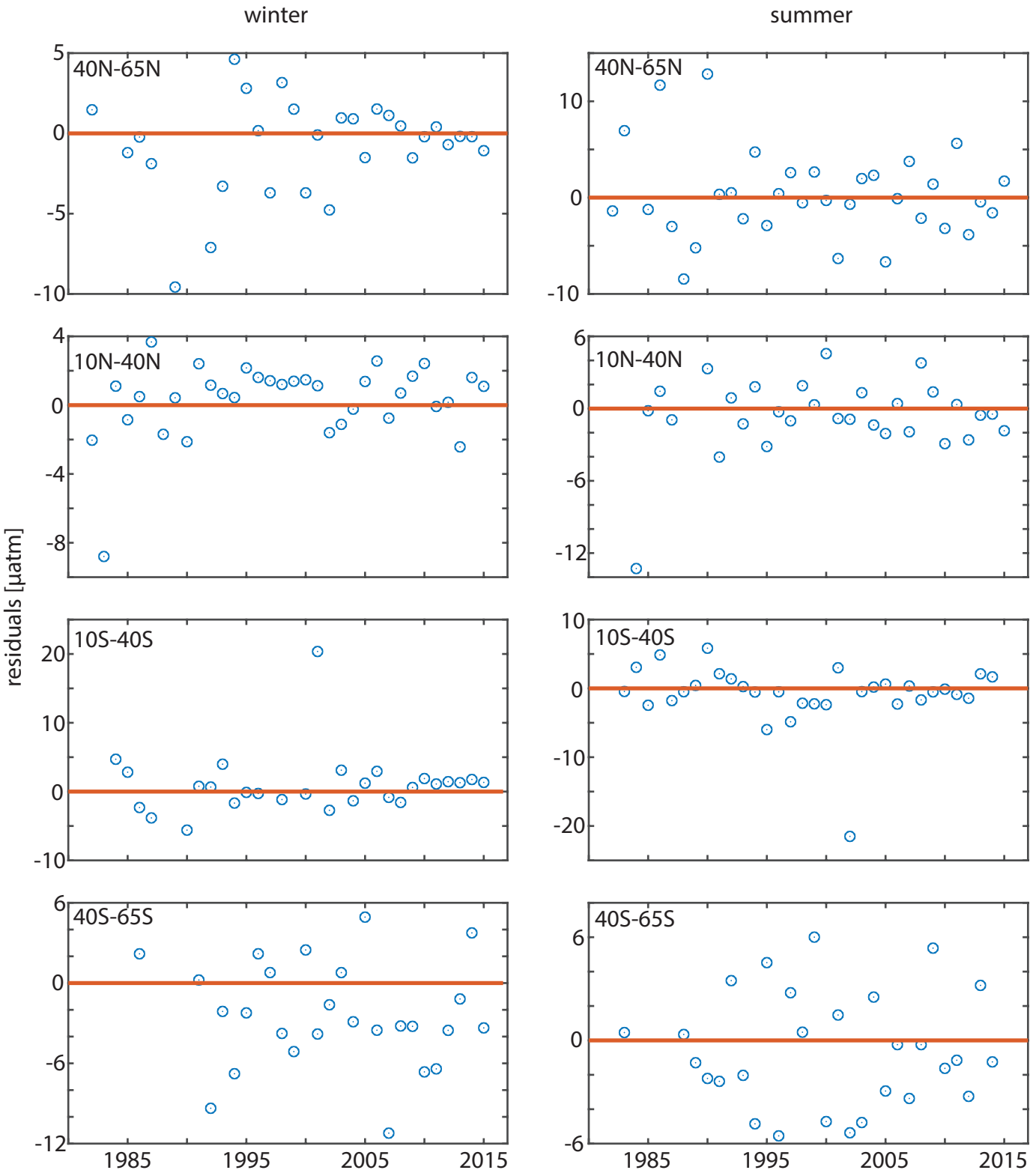
winter
summer
40N-65N
10N-40N
10S-40S
40S-65S
residuals [µatm]
1985
1995
2005
2015

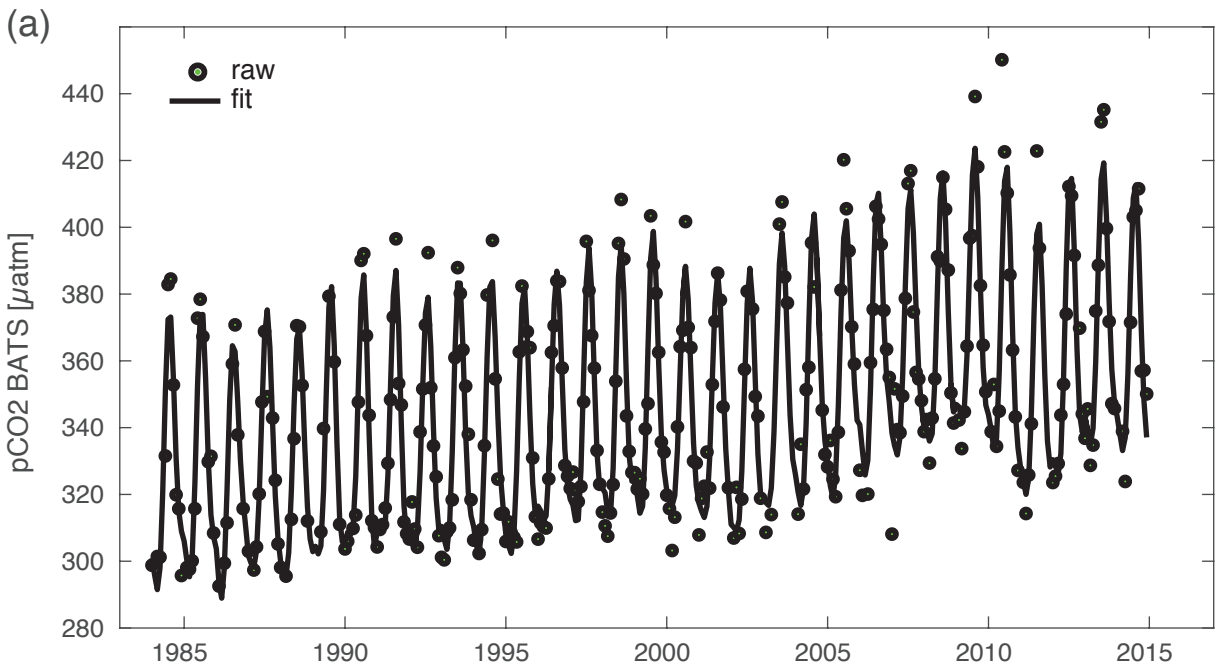
(a)
raw
fit
pCO2 BATS [μatm]
440
420
400
380
360
340
320
300
280
1985
1990
1995
2000
2005
2010
2015

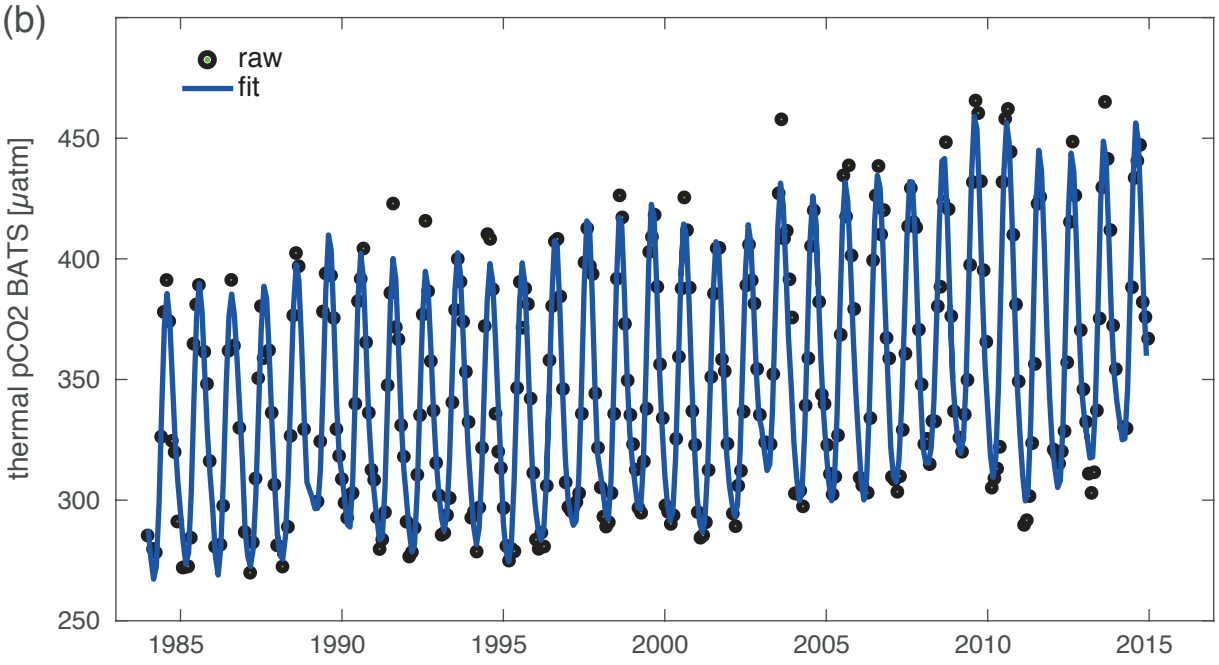
(b)
raw
fit
thermal pCO2 BATS [μatm]
450
400
350
300
250
1985
1990
1995
2000
2005
2010
2015

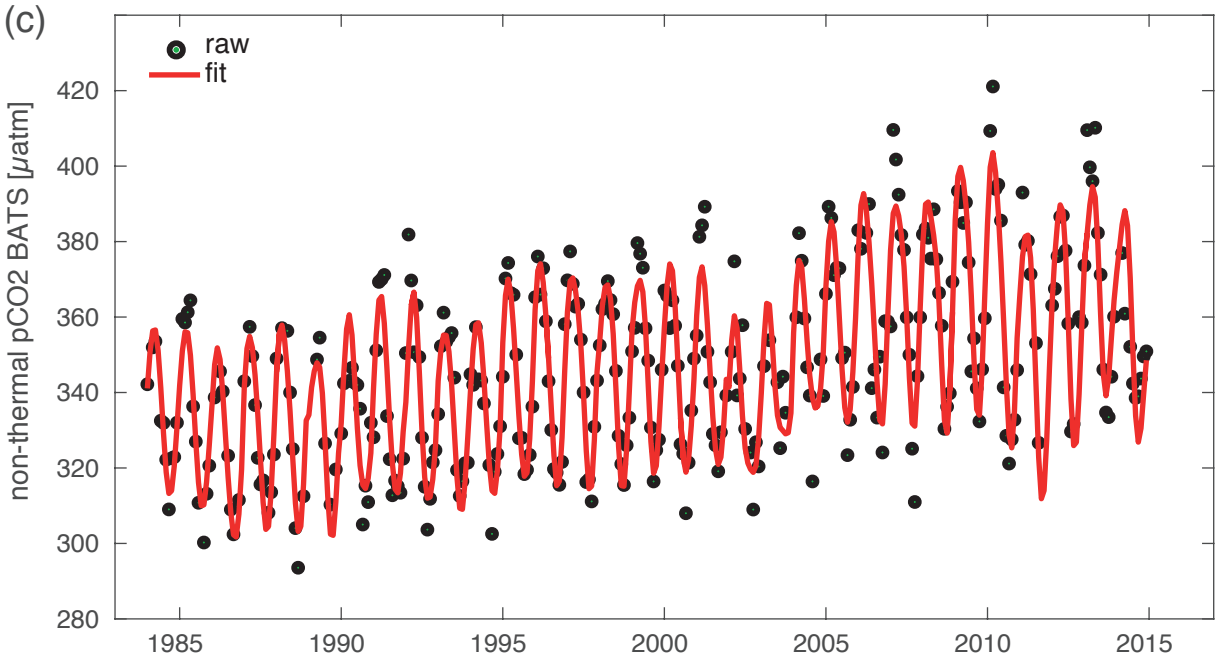
(c)
raw
fit
non-thermal pCO2 BATS [μatm]
420
400
380
360
340
320
300
280
1985
1990
1995
2000
2005
2010
2015

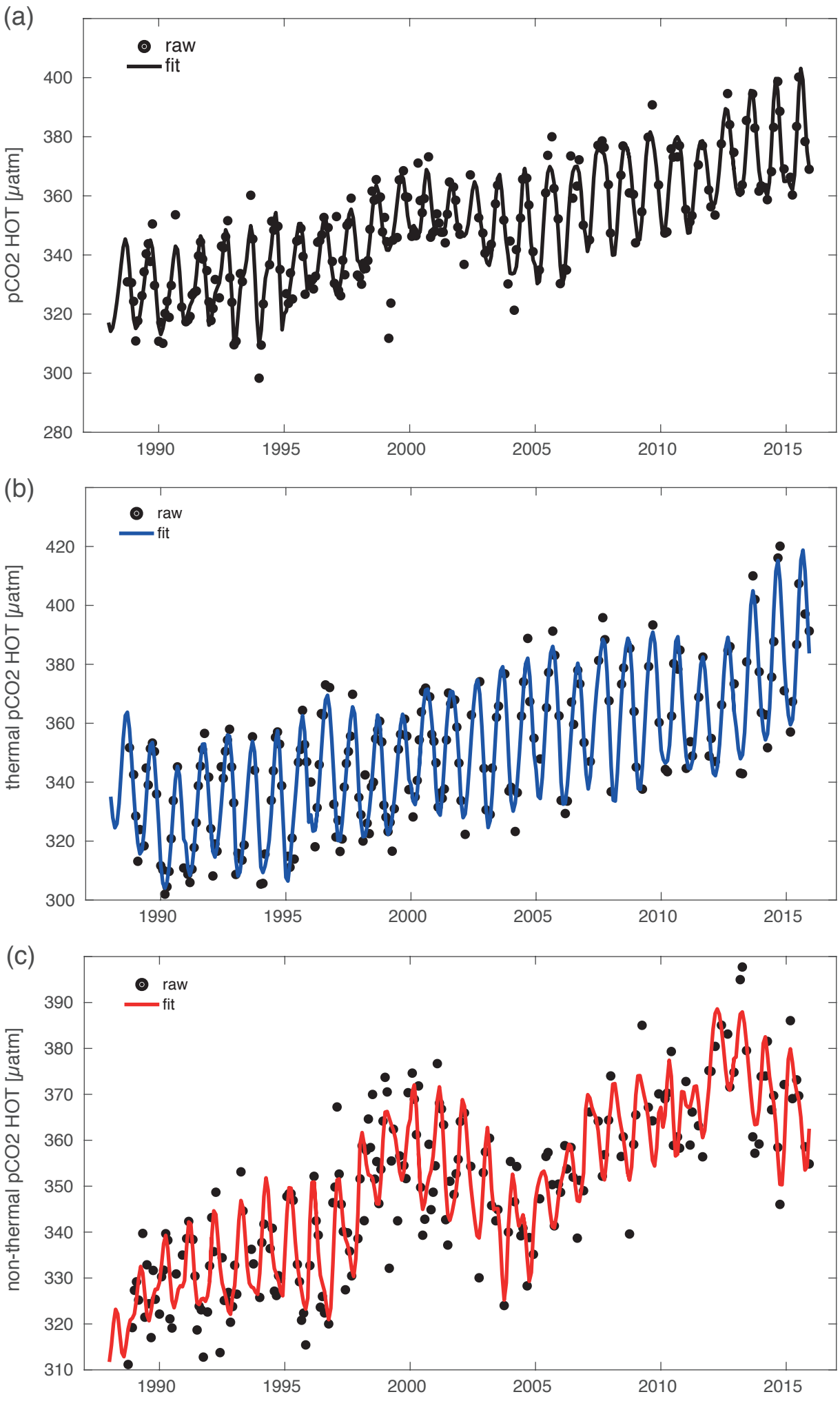
(a)
raw
fit
pCO2 HOT [µatm]
400
380
360
340
320
300
280
1990
1995
2000
2005
2010
2015
(b)
raw
fit
thermal pCO2 HOT [µatm]
420
400
380
360
340
320
300
1990
1995
2000
2005
2010
2015
(c)
raw
fit
non-thermal pCO2 HOT [µatm]
390
380
370
360
350
340
330
320
310
1990
1995
2000
2005
2010
2015

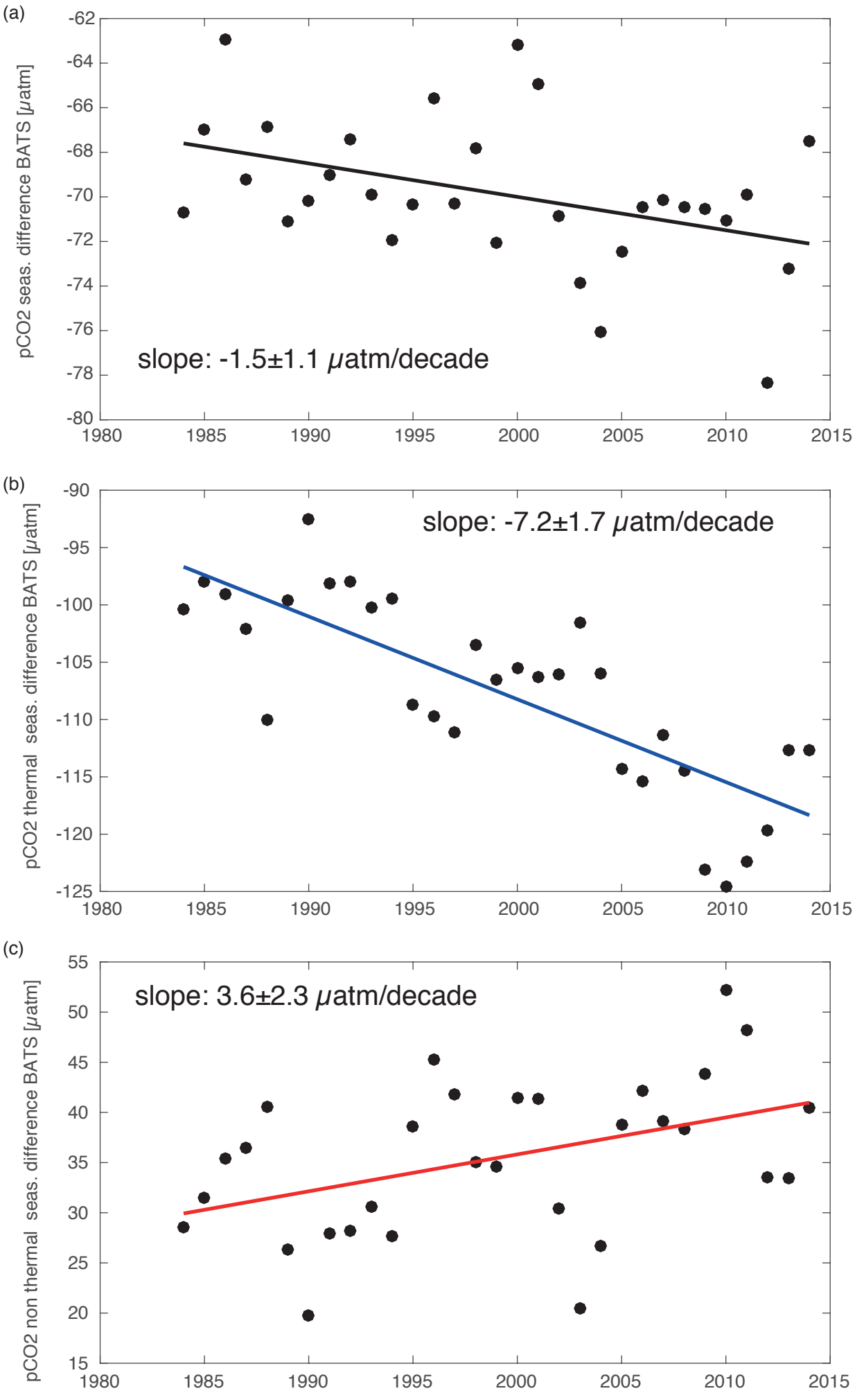
(a)
pCO2 seas. difference BATS [μatm]
-62
-64
-66
-68
-70
-72
-74
-76
-78
-80
1980
1985
1990
1995
2000
2005
2010
2015
slope: -1.5±1.1 μatm/decade
(b)
pCO2 thermal seas. difference BATS [μatm]
-90
-95
-100
-105
-110
-115
-120
-125
slope: -7.2±1.7 μatm/decade
(c)
pCO2 non thermal seas. difference BATS [μatm]
55
50
45
40
35
30
25
20
15
slope: 3.6±2.3 μatm/decade

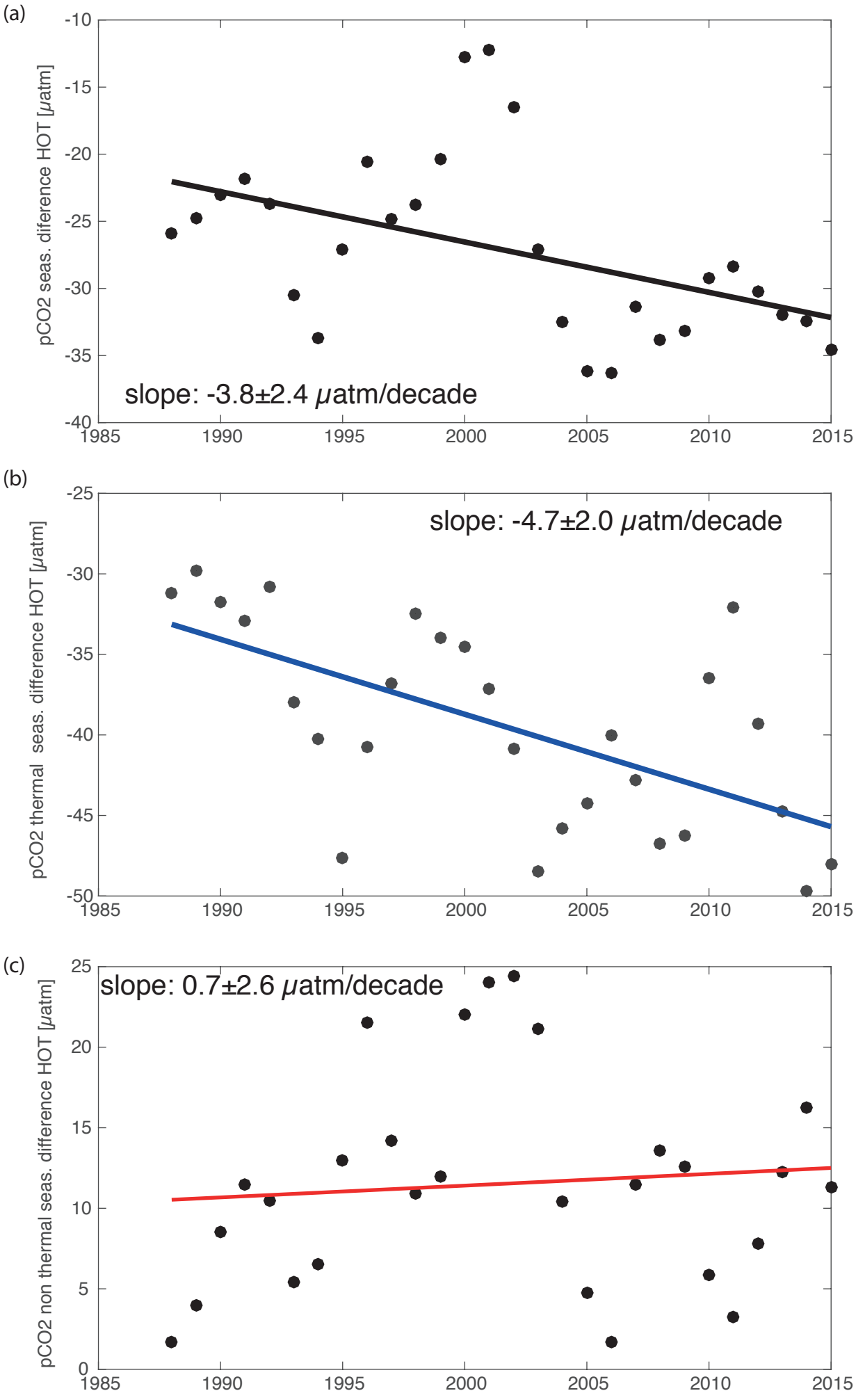
(a)
pCO2 seas. difference HOT [μatm]
slope: -3.8±2.4 μatm/decade
(b)
pCO2 thermal seas. difference HOT [μatm]
slope: -4.7±2.0 μatm/decade
(c)
pCO2 non thermal seas. difference HOT [μatm]
slope: 0.7±2.6 μatm/decade
1985
1990
1995
2000
2005
2010
2015

(a) Atlantic Ocean

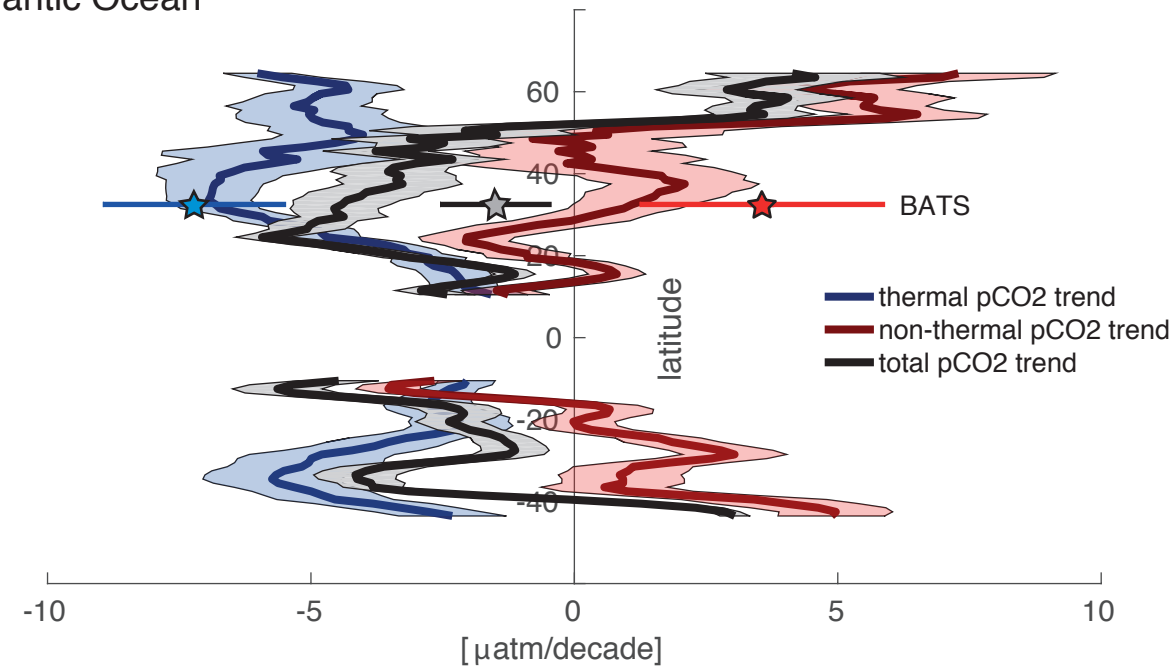

(b) Pacific Ocean

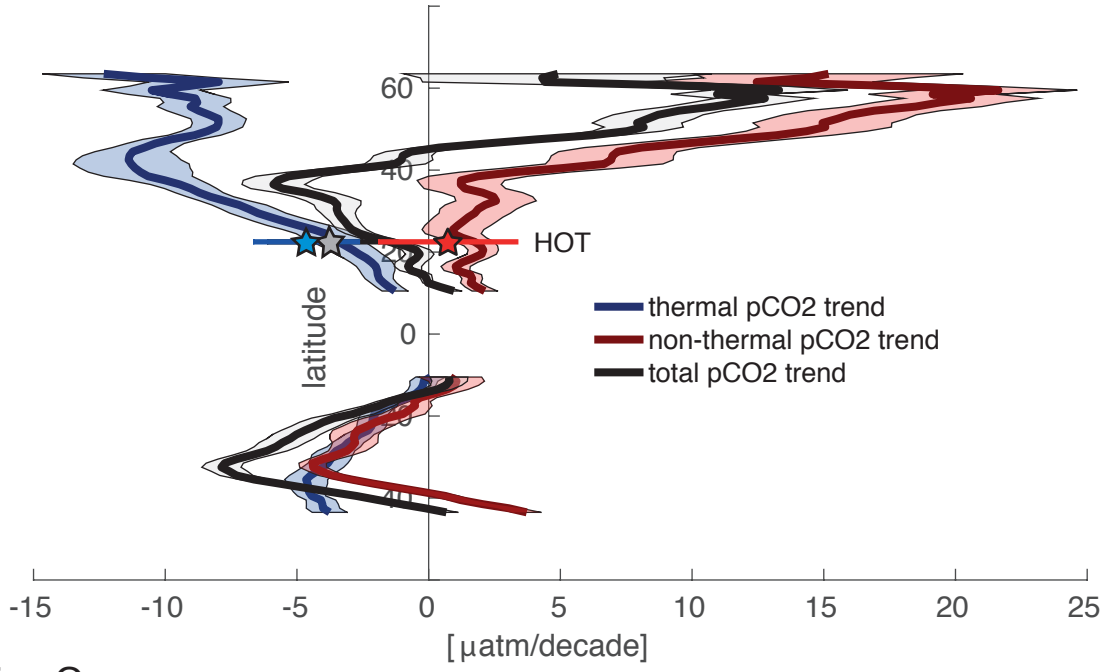

(c) Indian Ocean

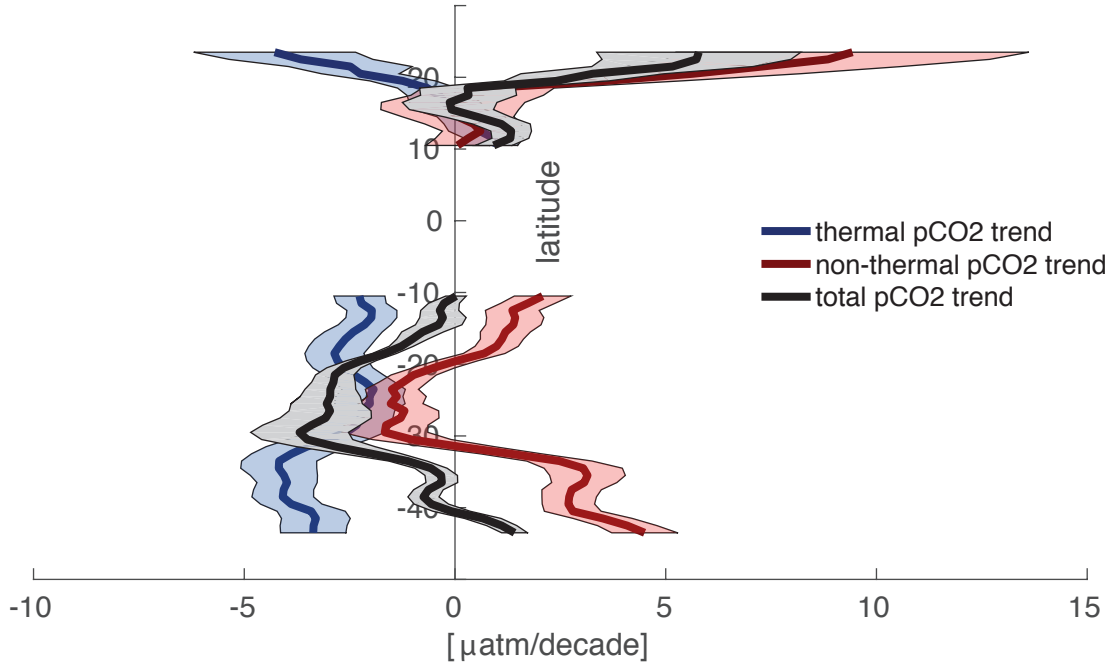

(a)

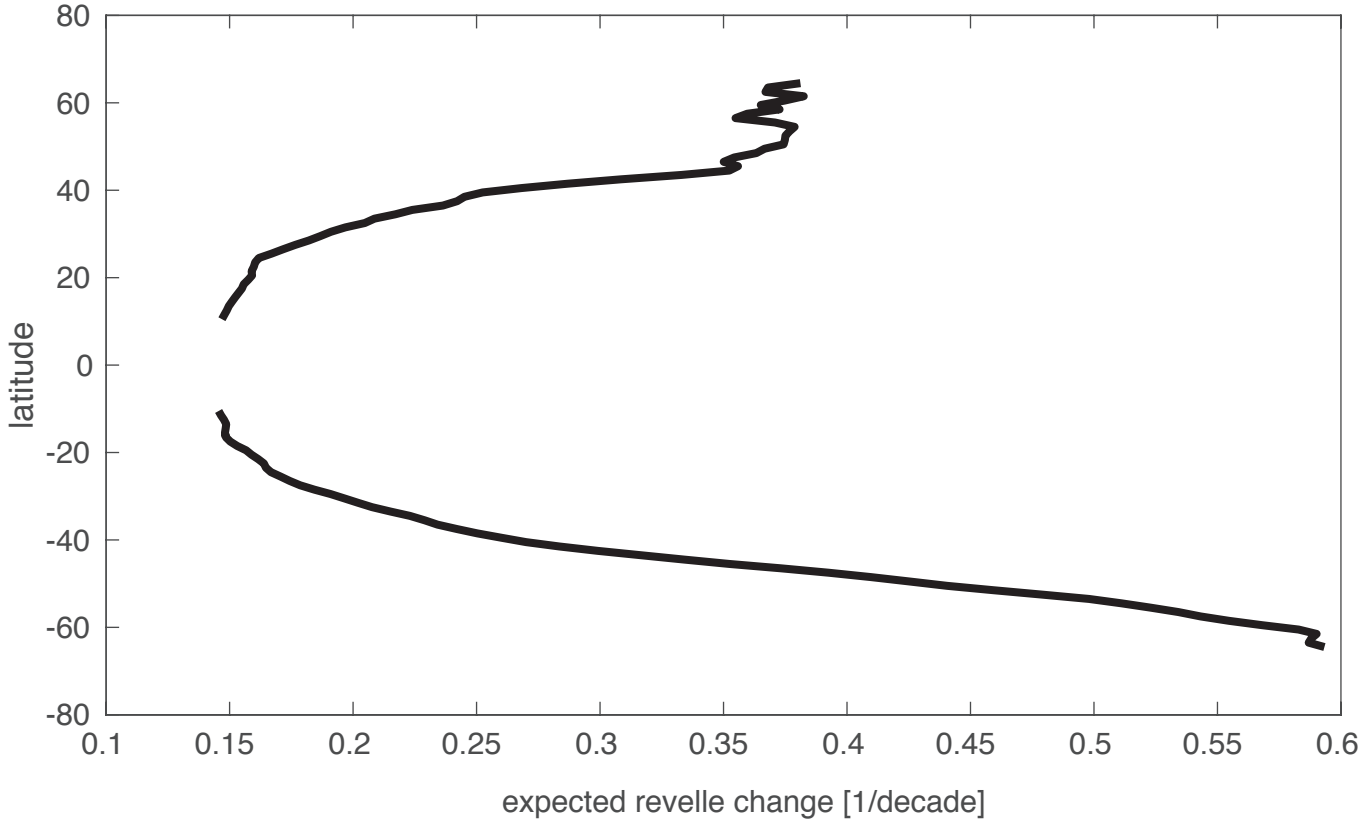
80
60
40
20
0
-20
-40
-60
-80
latitude
0.1
0.15
0.2
0.25
0.3
0.35
0.4
0.45
0.5
0.55
0.6
expected revelle change [1/decade]

(b)

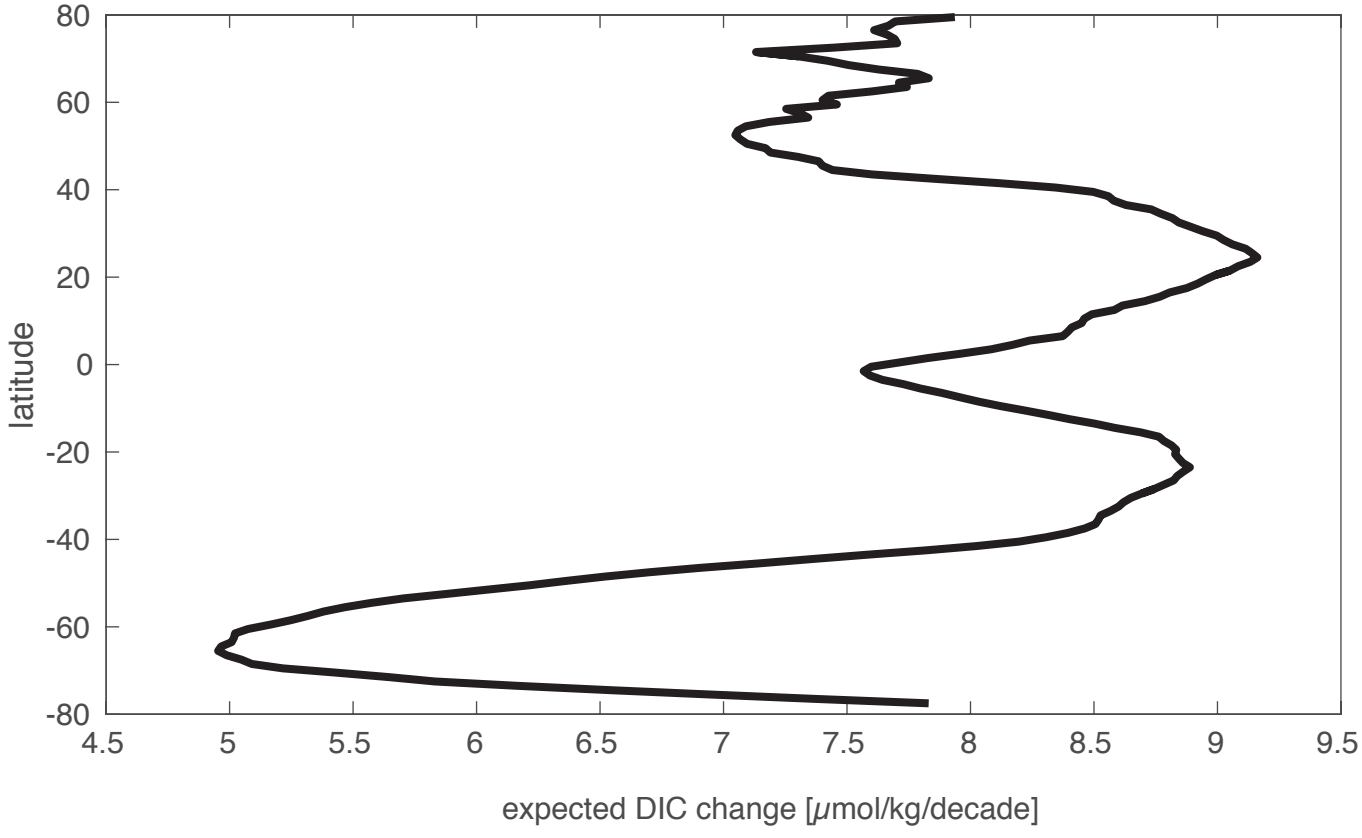
80
60
40
20
0
-20
-40
-60
-80
latitude
4.5
5
5.5
6
6.5
7
7.5
8
8.5
9
9.5
expected DIC change [μmol/kg/decade]

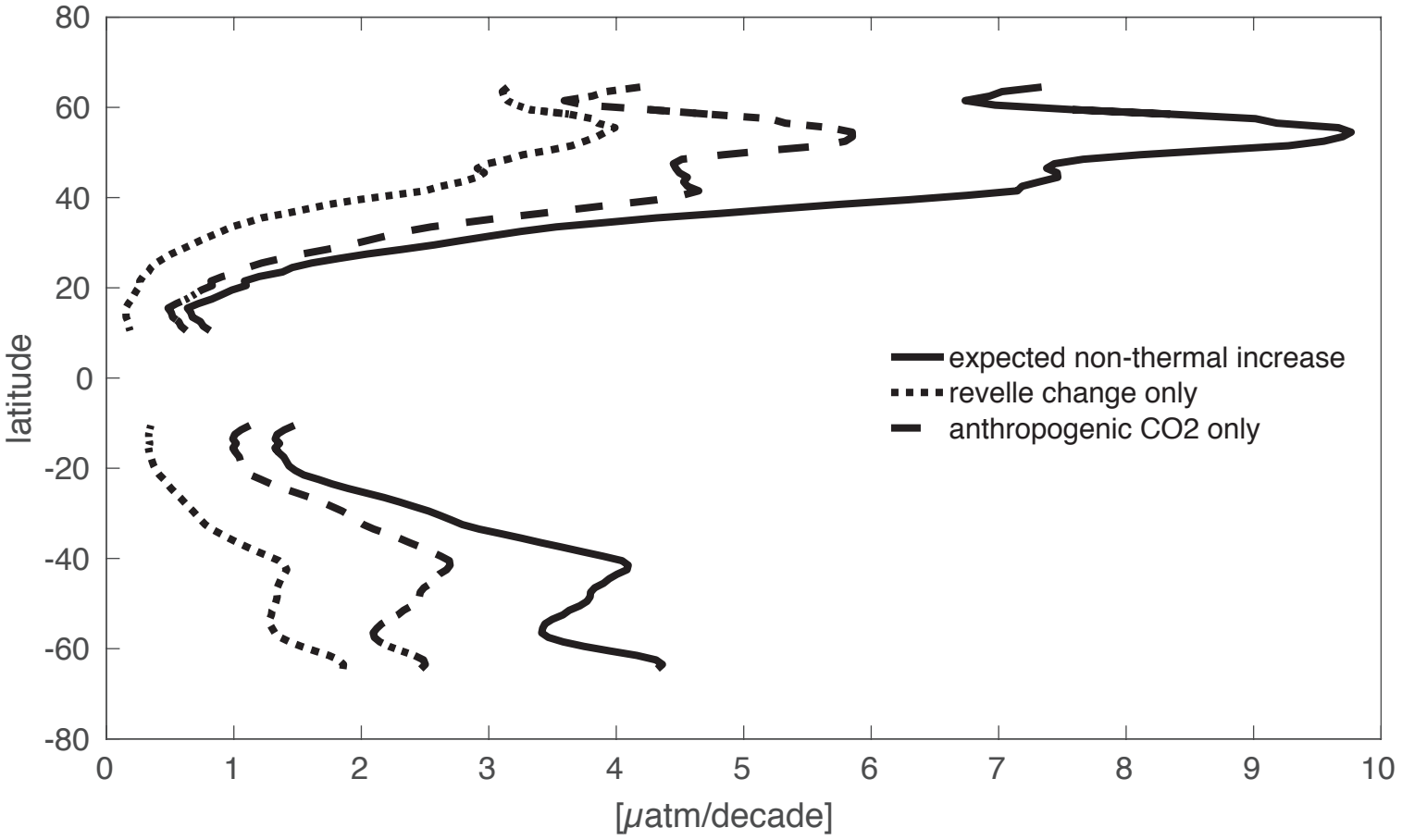
80
60
40
20
0
-20
-40
-60
-80
latitude
0
1
2
3
4
5
6
7
8
9
10
[μatm/decade]
expected non-thermal increase
revelle change only
anthropogenic CO2 only

(a) Atlantic Ocean

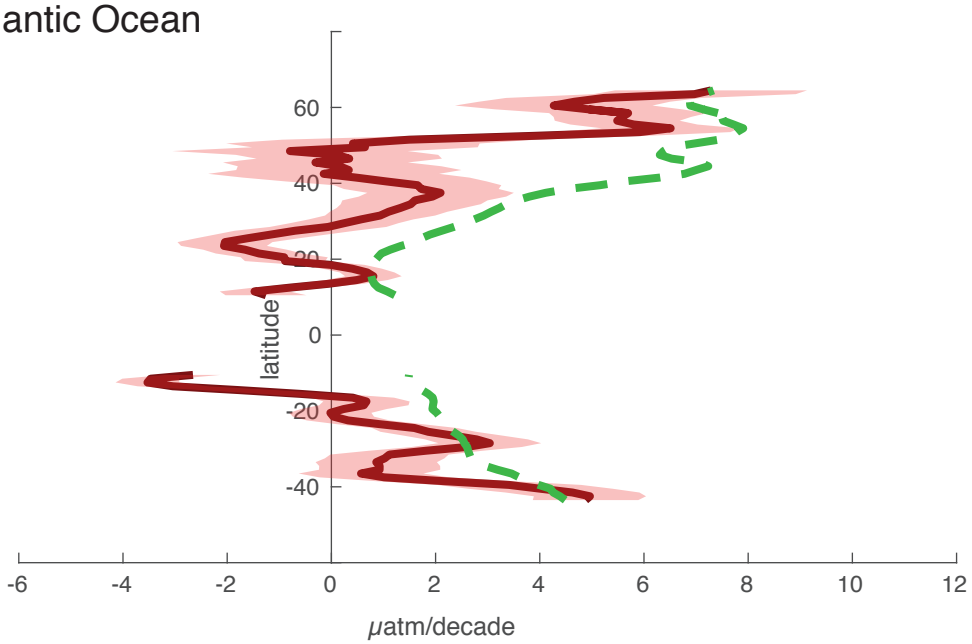

(b) Pacific Ocean

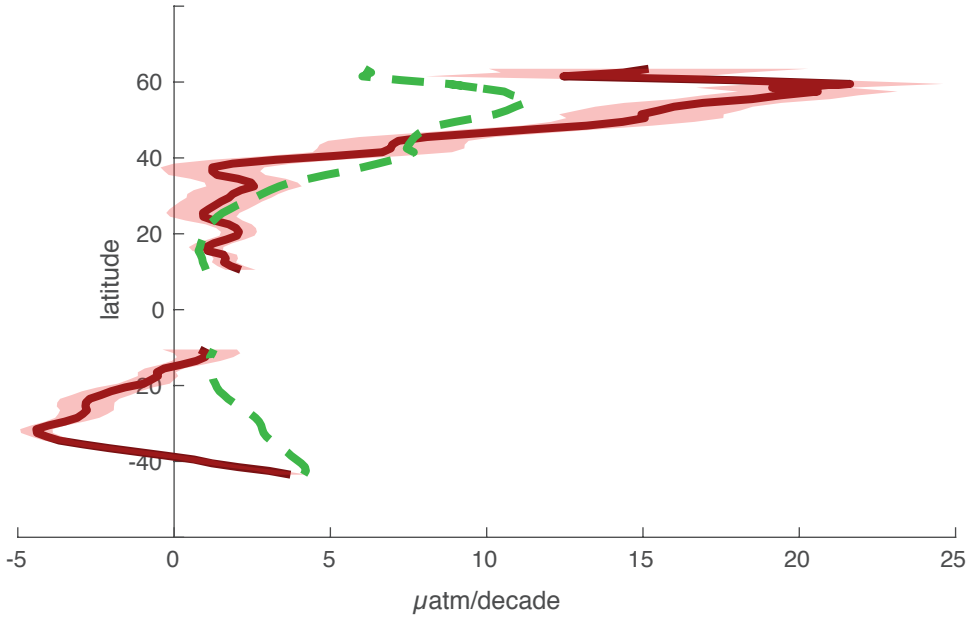

(c) Indian Ocean